

Numerical Simulation of Neutron Radiation Effects in Avalanche Photodiodes

Mark D. Osborne, Peter R. Hobson, and Stephen J. Watts

Abstract—A new one-dimensional (1-D) device model developed for the simulation of neutron radiation effects in silicon avalanche photodiodes is described. The model uses a finite difference technique to solve the time-independent semiconductor equations across a user specified structure. The model includes impact ionization and illumination allowing accurate simulation with minimal assumptions. The effect of neutron radiation damage is incorporated via the introduction of deep acceptor levels subject to Shockley-Read-Hall statistics. Preliminary analysis of an EG&G reverse APD structure is compared with experimental data from a commercial EG&G C30719F APD.

Index Terms—Avalanche photodiodes, numerical analysis, neutron radiation effects.

I. INTRODUCTION

HIGH-ENERGY physics experiments at the Large Hadron Collider (LHC) at CERN will operate in extremely harsh radiation environments. One of the experiments, the Compact Muon Solenoid (CMS), will operate in a 4 T magnetic field. The Electromagnetic Calorimeter (ECAL) is a vital subsystem of the CMS detector that uses scintillating PbWO₄ crystals to detect high energy electrons and photons. The crystals, chosen for their high density and radiation tolerance, have a low light yield that requires a photodetector with internal gain. The 4 T magnetic field excludes most vacuum photodetectors, leaving solid-state avalanche photodiodes (APD) and vacuum phototriodes (VPT) as the main candidates. The large neutron flux produced in the detector, with an energy spectrum peaking at 1 MeV, will significantly degrade the APD performance, reducing the calorimeter resolution. The development of a radiation-tolerant device is essential to maintain the overall detector performance.

The selection of APD technology for scintillation detection in the CMS ECAL [1] initiated an extensive research and development program. The main effort focused on the experimental evaluation of the properties of candidate devices [2], [3] such that a suitable device could be found. A large amount of experimental data was generated but comparison with modeled data has been limited so far [4]. To restore the balance, a one-dimensional (1-D) device model was developed at Brunel University to allow simulation of silicon avalanche photodiodes.

To provide a useful comparison with measurements the model included generation terms for impact ionization and illumination. One of the most important topics investigated was the ef-

fect of neutron irradiation on the performance of the devices. Thus, the inclusion of damage to the silicon crystal was necessary. This was facilitated, for 1 MeV neutrons, by recent advances (Section IV) and implemented via the introduction of acceptor-like states situated deep in the bandgap.

The aim of this paper is to present an overview of the device model and then describe the main effects, i.e., impact ionization, illumination and neutron radiation damage, in more detail. Section II will examine the model in general including the form of the semiconductor equations employed and their solution using a finite difference technique. The generation terms relating to impact ionization and illumination will be discussed in Section III. Section IV studies the terms relating to neutron radiation damage and the physical basis of the damage mechanism. Section V will present some preliminary results. The free electron and hole distributions, electric field profile, dc gain and photosensitivity are calculated. Qualitative comparison is made with experimental data from a commercial EG&G C30719F reverse reach through APD.

The results demonstrate that the model can accurately calculate the internal parameters of an APD and produce data that can be directly compared with measurements. The effects of 1 MeV neutron irradiation on the gain and photosensitivity are also investigated. Conclusions will be drawn in Section VI.

II. OVERVIEW

The preliminary analysis was performed on a structure based on the EG&G C30626E reverse reach-through APD. This photodetector has been considered as a possible candidate for the CMS ECAL. The device, a modified form of the standard reach-through structure, is optimized for scintillation applications [5]. The exact doping profile was withheld by the manufacturer. This proved to be a major stumbling block as the device performance is acutely dependent on the internal structure. A reasonable approximation of the doping profile can be made from existing descriptions [2], [5]. A schematic of the structure is shown in Fig. 1.

The structure was created using a simple *drive in* diffusion process, where a fixed amount of dopant was diffused into the semiconductor surface. After the diffusion time had been selected the position dependent concentration was given by

$$C(x) = \frac{S}{\sqrt{\pi Dt}} \exp\left[-\frac{x^2}{4Dt}\right] \quad (1)$$

where

- S total amount of dopant per unit area;
- D diffusion coefficient (Table II);

Manuscript received April 27, 1999; revised September 2, 1999. The review of this paper was arranged by Editor P. K. Bhattacharya.

The authors are with the Department of Electronic and Computer Engineering, Brunel University, Uxbridge UB8 3PH, U.K. (e-mail: Mark.Osborne@Brunel.ac.uk).

Publisher Item Identifier S 0018-9383(00)01488-X.

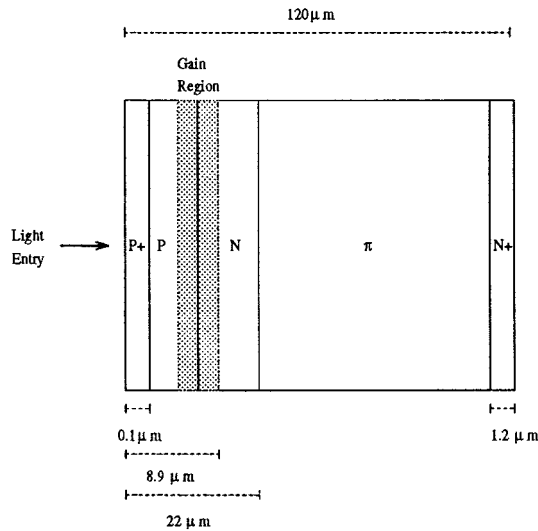


Fig. 1. Schematic of the proposed EG&G reverse reach-through APD type C30626E structure.

TABLE I
SPECIFICATIONS OF EACH OF THE
DIFFUSED IMPLANTS USED TO CREATE THE MODELLED C30626E STRUCTURE

Implant	S / cm^{-2}	t / s	Peak Level $/ \text{cm}^{-3}$	Depth $/ \mu\text{m}$
P+	1×10^{13}	5	3×10^{17}	0.12
P	9.4×10^{13}	4481	5×10^{16}	8.9
N	4.3×10^{13}	50206	8×10^{15}	22.0
N+	1×10^{14}	30	6×10^{17}	1.0
π	—	—	2.5×10^{12}	—

x position;

t diffusion time.

The parameters of the various implants are detailed in Table I.

The model utilized the basic methodology proposed in [6]. A 1-D static form was adequate to simulate the majority of the standard tests performed on APD's while retaining a level of simplicity that allowed new structures to be evaluated relatively quickly. The use of a 1-D model, compared with a more detailed two- or three-dimensional (2-D or 3-D) formulation, results in a significantly simplified approximation of the device behavior. Subsequently surface effects and nonuniformities along the lateral direction, which may result in avalanching outside the defined gain region, have to be ignored. Although we have to acknowledge that the model represents a very idealised version of an APD, it is still useful for investigating their behavior under neutron irradiation. The most significant effect of neutron irradiation is the change in the device characteristics along the path of the collected signal charge. Although there may be lateral variation in the magnitude of this effect, considering only the 1-D case still provides useful information about the change in the device's behavior.

The free carrier (electron and hole) concentration and electrostatic potential through the device were extracted from the model. The current density and electric field could subsequently be inferred. The current density provided the only route for direct comparison with measurements. When combined with the

external conditions, e.g., applied bias, quantities such as gain, dark current and photocurrent could be predicted. The electric field profile also provided useful information, e.g., multiplication factor, when analyzed appropriately.

The static semiconductor equations employed in the model were in the standard form

$$\frac{1}{q} \frac{dJ_p}{dx} - (G - U) = 0 \quad (2)$$

$$\frac{1}{q} \frac{dJ_n}{dx} + (G - U) = 0 \quad (3)$$

$$\frac{d^2\psi}{dx^2} = -\frac{q}{\epsilon} \left(\Gamma + p - n - \sum N_A \right). \quad (4)$$

\vec{J}_p and \vec{J}_n are the hole and electron current densities. G is a generation term consisting of impact ionization and the photoelectric generation of signal charge, and U is a thermal generation/recombination term. ψ is the electrostatic potential, Γ the net doping concentration, p and n are the free hole and electron concentrations and q the electronic charge. $\sum N_A$ represents the density of filled deep levels introduced during neutron irradiation. The density of filled acceptors, $\sum N_A$, is given by the product of the density of available levels, N_A , and the occupancy function, $f(E_T)$

$$\sum N_A = f(E_T) \times N_A. \quad (5)$$

The form of the occupancy function is described in more detail in Section IV. Inclusion of the occupancy function directly into the Poisson equation ensures that it is solved consistently with the Poisson and continuity equations across the whole device.

Application of finite differences involved dividing the device into a 1-D grid, each gridpoint containing information about the potential and free carrier (electron and hole) concentration. Efficient use was made of the grid by increasing the density of the gridpoints in the gain region of the device. The high potential gradient in this region requires an increased grid density to be accurately modeled. A typical array consisted of 2000 grid points, 1000 in the first 20% of the device surrounding the active region and the remaining 1000 spread uniformly across the final 80% of the device.

The semiconductor equations were expressed in a form consistent with the discrete nature of the grid, i.e., discretized, by expressing the spatial derivatives via a truncated Taylor series

$$\frac{dp}{dx} = \frac{p(N+1) - p(N)}{x(N+1) - x(N)}. \quad (6)$$

The discretized equations were solved via the application of Newton's iteration principle. This involved expressing the true value of each of the variables; carrier concentration and potential, in terms of the present value plus an associated increment, e.g., for holes

$$p_{\text{true}} = p_{\text{initial}}^0 + \delta p. \quad (7)$$

The individual terms in the equations were expanded via a truncated Taylor expansion in terms of the known value and associated increment e.g. for the hole current density

$$J_p(M)\{p(N), p(N+1), \psi(N), \psi(N+1)\} \\ = J_p^0(M) + \left[\delta p(N) \frac{\delta J_p^0(M)}{\delta p(N)} + \delta p(N+1) \frac{\delta J_p^0(M)}{\delta p(N+1)} \right. \\ \left. + \delta \psi(N) \frac{\delta J_p^0(M)}{\delta \psi(N)} + \delta \psi(N+1) \frac{\delta J_p^0(M)}{\delta \psi(N+1)} \right]. \quad (8)$$

The resulting set of linear equations was expressed as a tridiagonal matrix equation. Solution of the matrix equation, for the increment at each gridpoint, allowed the value of the fundamental variables to be amended. Hence, the solution to the discretized equations was improved. This process was repeated until the relative error at each gridpoint fell below a predetermined level. Generally a value of 5×10^{-9} was used as this was the limit that could be achieved for initial solutions.

The integral form of the current equation [8] was used to increase the stability of the solution in regions of high electric field [6] inherently present in an APD. The high grid density allowing the assumption that the electric field, mobility and current density were constant between grid points.

$$J_p = -\frac{q\mu_p E}{1 - e^{\theta Ex}} [p(0)e^{\theta Ex} - p(x)] \quad (9)$$

$$J_n = -\frac{q\mu_n E}{1 - e^{-\theta Ex}} [n(0)e^{-\theta Ex} - n(x)] \quad (10)$$

where μ_p and μ_n are the hole and electron mobilities, E the electric field, and θ represents q/kt .

To initiate the process a preliminary solution was provided. Assuming space charge neutrality the initial carrier densities were given by

$$\left. \begin{array}{l} p = -\Gamma \\ n = -\frac{n_i^2}{\Gamma} \end{array} \right\} P \text{ region} \quad (11)$$

$$\left. \begin{array}{l} p = \frac{n_i^2}{\Gamma} \\ n = \Gamma \end{array} \right\} N \text{ region.} \quad (12)$$

The potential, with no external bias was set to be

$$\frac{1}{\theta} \ln\left(-\frac{n_i}{\Gamma}\right) \left\} P \text{ region} \quad (13)$$

$$\frac{1}{\theta} \ln\left(\frac{\Gamma}{n_i}\right) \left\} N \text{ region.} \quad (14)$$

It was assumed that the device had ideal ohmic contacts, i.e., they were at thermal equilibrium; hence, any excess charge immediately vanished and no space charge existed. It was thought that neglect of effects due to space charge or electric field at the contacts was justified. The device structures were created assuming simple diffusion profiles, which were used to generate the initial trial solution.

TABLE II
VALUES OF THE MAIN PARAMETERS USED IN THE MODEL AT 300 K

Parameter	Value at 300K	Reference
n_i	$1.48 \times 10^{10} \text{cm}^{-3}$	[6]
τ_0	100 μs	[16]
E_g	1.12 eV	[14]
D_P	(Phosphorus diffusion coeff. at 1200°C)	[7]
	$3.0 \times 10^{-12} \text{cm}^2 \text{s}^{-1}$	
D_B	(Boron diffusion coeff. at 1200°C)	[7]
	$4.5 \times 10^{-12} \text{cm}^2 \text{s}^{-1}$	

TABLE III
CONSTANTS USED IN THE PARAMETERIZATION OF THE CARRIER MOBILITY

Constant	μ_p	μ_n
$N_{ref} \text{ (cm}^{-3}\text{)}$	6.3×10^{16}	8.5×10^{16}
α	0.76	0.72
$\mu_{hi} \text{ (cm}^2 \text{V}^{-1} \text{s}^{-1}\text{)}$	495	1330
$\mu_{lo} \text{ (cm}^2 \text{V}^{-1} \text{s}^{-1}\text{)}$	47.7	65
$E_c \text{ (Vcm}^{-1}\text{)}$	1.95×10^4	8×10^3
β	1	2

A list of the main parameters used in the simulation is provided in Table II. The mobility was calculated at each gridpoint according to

$$\mu = \frac{\mu_{hi} - \mu_{lo}}{1 + \left(\frac{|N|}{N_{ref}}\right)^\alpha + \left[\frac{(\rho n)^{\frac{1}{2}}}{2.04N_{ref}}\right]^\alpha} \times \frac{1}{\left[1 + \left(\frac{E}{E_c}\right)^\beta\right]^{\frac{1}{\beta}}}. \quad (15)$$

The values of the constants are listed in Table III.

III. IMPACT IONIZATION AND ILLUMINATION

The process of impact ionization, a pre-condition for the operation of an APD, was incorporated into the continuity equations via a generation term

$$G = \frac{1}{q} (\alpha_n J_n + \alpha_p J_p) \quad (16)$$

where α_p and α_n are the hole and electron ionization rates, respectively. A modified [9] form of the Baraff three parameter theory [10] was used to calculate the ionization rates in silicon.

$$\alpha_{p/n} = \frac{1}{\lambda_{p/n}} \exp\left(\frac{A\varepsilon_i^2}{e^2 E^2 \lambda_{p/n}^2} + \frac{B\varepsilon_i}{eE\lambda_{p/n}} + C\right) \quad (17)$$

$$\begin{aligned} A &= 11.5r^2 - 1.17r + 3.9 \times 10^{-4} \\ B &= 46r^2 - 11.9r + 1.75 \times 10^{-2} \\ C &= -757r^2 + 75.5r - 1.92 \end{aligned} \quad (18)$$

$$r = \frac{\langle \varepsilon_r \rangle}{\varepsilon_i}. \quad (19)$$

Following [10], ε_i , the activation energy, is taken to be $3E_G/2$ where E_G is the bandgap energy, $\langle \varepsilon_r \rangle$ is the mean energy loss per optical phonon collision. $\lambda_{p/n}$ is the optical phonon mean

free path for either holes or electrons. Following [11], the variation of ionization rate with temperature was accounted for via the expressions

$$\langle \varepsilon_r \rangle = \varepsilon_r \tanh\left(\frac{\varepsilon_r}{2kT}\right) \quad (20)$$

$$\lambda = \lambda_0 \tanh\left(\frac{\lambda_0}{2kT}\right) \quad (21)$$

where λ_0 is taken to be 55 Å for holes and 76 Å for electrons and ε_r , 0.063 eV.

The modified Baraff three parameter theory was successfully used to model temperature effects in EG&G silicon APD's [13]. Sutherland developed a more accurate empirical fit to the Baraff curves [11]. This provides a good fit to the Baraff curves over a wider range of parameter values than the Crowell–Sze approximation [9]. The disadvantage of the Sutherland method is that the resulting parameterization has a cubic form. Incorporating this technique into the model would increase the complexity dramatically, hence reducing the computational efficiency. At 300 K and up to electric fields of around 300 kVcm⁻¹, approximately the maximum reached in the model, the less complex Crowell–Sze approximation performs equally well to the Stephenson model. Hence, the use of the Crowell–Sze approximation is preferable due to its relative simplicity.

Monochromatic illumination was included via a generation term in the continuity equations. Normal incidence was assumed at all times.

$$G = e^{-\beta x(N)} - e^{-\beta x(N+1)}. \quad (22)$$

Here, β represents the optical absorption coefficient in silicon. The signal charge generated at each gridpoint represented the integrated charge generated over the whole intergridpoint spacing. The variation in optical absorption coefficient with wavelength in silicon was parameterised using data from [15]. Thus monochromatic light of varying intensity and wavelength could be accurately modeled.

IV. FAST NEUTRON RADIATION DAMAGE

Recent advances have been made in the understanding of the processes involved in neutron radiation damage to silicon devices [16]–[18], although few are directly related to APD's. Vacancy (V) and interstitial (I) type defects are created in the semiconductor lattice for many types of irradiation. The significant difference between fast neutron radiation and, for example, ⁶⁰Co γ irradiation arises due to the large amount of energy imparted to the primary knock-on atom (PKA). The recoiling PKA goes on to create a large cluster of V and I defects (a ⁶⁰Co γ will only cause at most two silicon atoms to be displaced). The majority of these defects recombine immediately, the rest either form divacancies (V₂) or higher order V complexes; or the defects diffuse into the lattice and combine with impurity atoms. The introduction rate is defined as the rate at which defects are introduced per unit neutron flux. For 1 MeV neutron irradiation, the introduction rate for the divacancy (V₂) is approximately 100 times greater than for ⁶⁰Co γ irradiation [18].

One of the most significant effects produced by radiation damage is the change in the effective doping concentration [19]. It was observed that for n-type diodes the value of N_{eff} , measured from the depletion voltage, initially fell with 1 MeV neutron fluence until the device became p-type. The fluence at which this occurs is known as the *inversion fluence*. N_{eff} then increased linearly with neutron fluence at a rate of 0.016 cm⁻¹.

Initially, for fluences below the *inversion fluence*, this was attributed to the combination of vacancy (V) defects with the phosphorus dopant atoms, producing the well-known *E*-center in silicon. It was discovered by Watts *et al.* that the removal rate of phosphorus in microstrip diodes was approximately 30 times lower than the level required to produce the measured change in N_{eff} [16]. A new theory was thus developed that attributed the change in N_{eff} to the creation of acceptor-like states deep in the bandgap [16]. It was known that, at thermal equilibrium, the devices became intrinsic after heavy neutron irradiation. The change in N_{eff} occurred in the intrinsic region only when the diode was reverse biased. The change in the effective doping concentration is thus a consequence of the space-charge distribution produced by the ionised deep levels.

Neutron damage was incorporated into the model via the introduction of deep acceptor levels. This method was successfully used to model the change in N_{eff} with neutron fluence [16]. The deep levels were filled using a Shockley–Read–Hall occupancy function where the fraction of filled acceptors, at energy E_T and gridpoint N , was given by

$$f(E_T, N) = \frac{n(N) + \frac{\sigma_p}{\sigma_n} n_i \exp\left(\frac{E_i - E_T}{kT}\right)}{n(N) + p(N) \frac{\sigma_p}{\sigma_n} + n_i \exp\left(\frac{E_T - E_i}{kT}\right) + \frac{\sigma_p}{\sigma_n} n_i \exp\left(\frac{E_i - E_T}{kT}\right)} \quad (23)$$

where σ_p and σ_n are the hole and electron capture cross sections. The most likely candidate for the deep acceptor level is the V₂O complex [20], [21] which is situated 0.5 eV below the conduction band. The introduction rate, for 1 MeV neutrons, has been calculated from a defect kinematics model to be 0.96 cm⁻¹ at 20°C [21].

The increase in dark current during neutron irradiation is due to the introduction of recombination centers with energy levels deep in the bandgap. This leads to an increase in the thermal generation of charge carriers. This process is described in the simulation via the modification of the minority carrier lifetime, τ , which controls the Shockley–Read–Hall thermal generation/recombination term in the continuity equations. The variation in minority carrier lifetime, τ , with neutron fluence, Φ_n in silicon under equilibrium conditions, was described in terms of the lifetime damage-constant, K_τ [22]

$$\frac{1}{\tau} = \frac{1}{\tau_0} + \frac{\Phi_n}{K_\tau}. \quad (24)$$

For high fluences, this could be written as

$$\frac{1}{\tau} \approx \frac{\Phi_n}{K_\tau}. \quad (25)$$

The value of K_τ was calculated for high resistivity-silicon [22] to be approximately $K_\tau = 10^7$ scm⁻². It was assumed that the

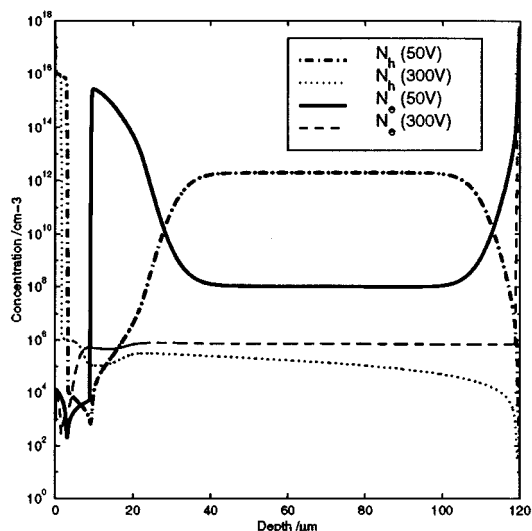


Fig. 2. Free hole and electron distribution through the modeled APD for bias voltages of 50 and 300 V. The device is undepleted at 50 V and fully depleted at 300 V.

effective carrier lifetime in the depletion region was subject to the same relation. With K_τ set to 10^7 scm^{-2} the rate of change of N_{eff} with fluence was kept consistent with predictions [20], [22] by setting the ratio of the hole and electron capture cross sections to unity [20].

The introduction of the deep acceptor level was assumed to be linear with neutron fluence. To limit the complexity of the preliminary analysis, annealing was not included.

V. RESULTS

The results included in this report are divided into two key sections; pre-irradiation and post-irradiation. They are intended to introduce possible avenues of investigation available to the model. All the neutron fluences have been normalized to 1 MeV neutrons. Qualitative comparison is made using Experimental data from a commercial EG&G C30719F reverse reach through APD. This device has a similar structure to the EG&G C30626E APD proposed for use in the CMS ECAL. To account for the slight difference in doping profile between the C30626E and the C30719F, resulting in the C30719F fully depleting at a bias 20 V greater than the C30626E, the simulation data is shifted 20 V along the x axis. Detailed knowledge of the doping profile will be required before quantitative comparisons can be made with experimental data.

A. Pre-Irradiation

For high efficiency the APD is generally operated with a high reverse bias, typically around 300 V to 400 V. The large drift velocity in the depleted region allows rapid collection of the signal charge. Fig. 2 shows the change in electron and hole distribution with reverse bias. A high reverse bias is required to produce significant depletion in the device, due to the highly doped p^+ region. Depletion through the π region occurs much more readily, to leave the majority of the device depleted.

Fig. 3 shows the potentials and electric fields through the device vary with depth for 50 V and 300 V. When fully

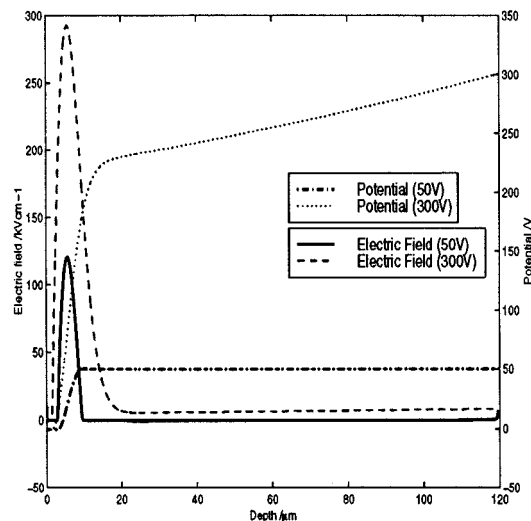


Fig. 3. The electric field and potential profile through the modeled APD. The device is undepleted at 50 V and fully depleted at 300 V.

depleted the pn junction contains an electric field sufficient to cause impact ionization, this region is responsible for the gain in the device. The multiplication factor of the device is defined as the total number of charges produced by a single charge injected into the gain region. In general, silicon APD's are designed to inject electrons into the gain region as this helps to reduce noise. The C30626E is no exception, and thus we only need consider the electron multiplication factor, M_e . This can be found by evaluating the following expression across the depleted region (of width w):

$$M_e = \frac{1}{1 - \int_0^w \alpha_n \exp^{-\int_0^x \alpha_n - \alpha_p dx'} dx}. \quad (26)$$

The response of avalanche photodiodes to different wavelengths of light is complicated by the structure of the gain region. A significant amount of signal charge may be generated inside the gain region as the wavelength of the incident light increases. These charge carriers undergo less multiplication than those created outside the gain region. Thus the apparent gain, i.e., the true gain experienced by an incident signal of a particular wavelength, will differ from the multiplication factor of the device.

Fig. 4 compares the apparent gain, calculated from the model with measurements of the DC gain from an EG&G C30719F APD at several incident wavelengths. The data from the model is shifted 20 V along the x axis to aid the comparison. The apparent gain is found by employing a commonly-used experimental method. The device is illuminated; subtraction of the dark current gives the photocurrent. An unmultiplied reference photocurrent is found by selecting a bias for which there is approximately unity gain but enough depletion to effectively collect the signal charge and not perturb the quantum efficiency. The current gain is defined as the ratio of the photocurrent at an arbitrary bias to the reference photocurrent.

The data in Fig. 4 displays the characteristic knee that can be seen in most reach-through devices. This marks the point where the depletion has spread into the π region. After this point there is a significant potential drop over the bulk of the device, Fig. 3,

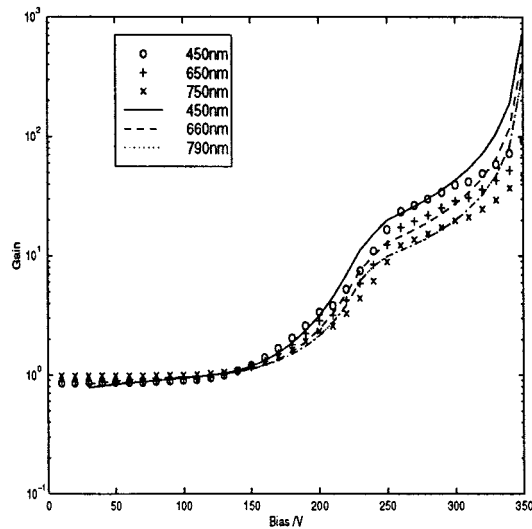


Fig. 4. Comparison of the predicted change in gain with incident wavelength for a modeled EG&G C30626E (line) with measurements performed on an EG&G C30719f APD (data points).

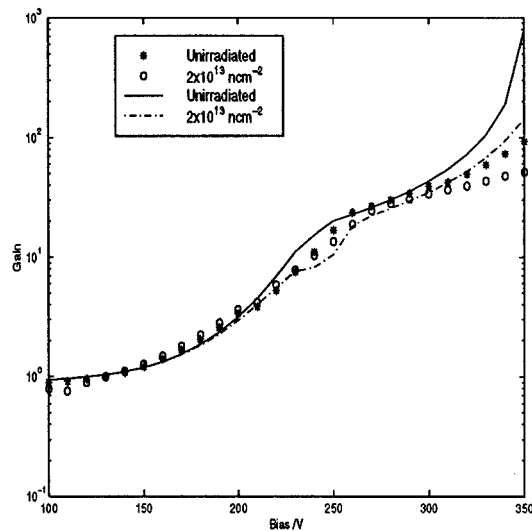


Fig. 5. Comparison of the predicted change in gain with neutron irradiation for an EG&G C30626E APD at 450 nm (lines) with measurements performed on an EG&G C30719F APD at 450 nm (data points), annealing is ignored.

and the sensitivity of the potential gradient to the applied bias in the gain region is reduced.

B. Post-Irradiation

Fig. 5 compares the fall in gain with neutron fluence, predicted by the model with measurements taken from an EG&G C30719F APD. The data from the model is shifted 20 V along the x axis to aid the comparison. Although a quantitative comparison between the predicted and measured data is not possible, as a result of the structural uncertainty the model shows good qualitative agreement. This effect has been observed by several groups [23]. This can be attributed to a reduction in the electric field around the gain region of the device due to space charge from the filled deep acceptor levels. Fig. 6 shows our prediction

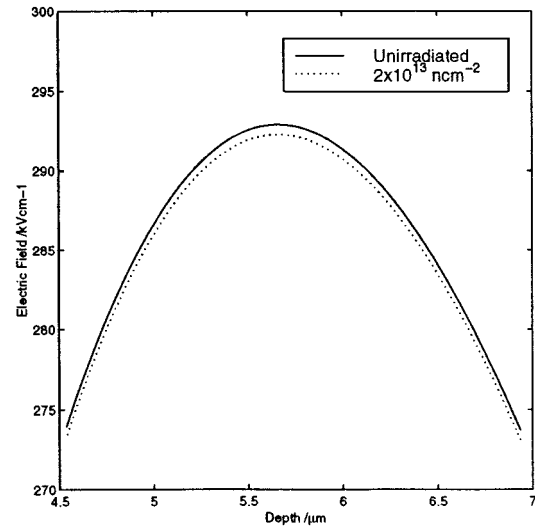


Fig. 6. Effect of neutron irradiation on the electric field in the vicinity of the gain region at 300 V, showing that the multiplying power of the device is degraded, annealing is ignored.

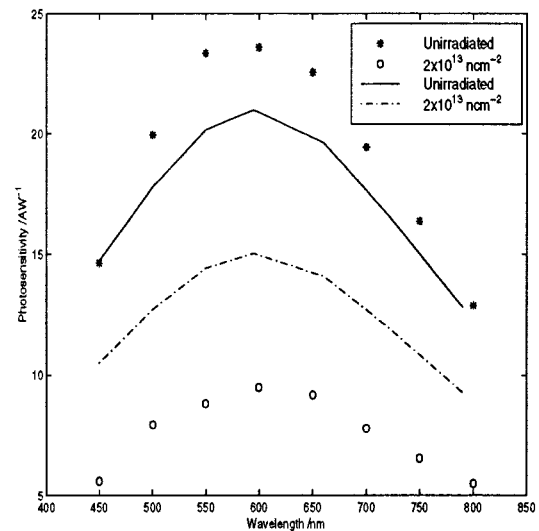


Fig. 7. Comparison of the predicted change in photosensitivity with neutron irradiation for an EG&G C30626E APD (lines) with measurements performed on an EG&G C30719F APD (data points) at a gain of 40, annealing is ignored.

of how the electric field in the gain region is affected by neutron irradiation. The fall in the electric field demonstrates that the gain degradation is actually a reduction in the *multiplying power* of the device and not due to a change in the charge collection efficiency.

The photosensitivity of a device is defined as the ratio of photocurrent per incident Watt of power in the same area. Fig. 7 compares the calculated effect of neutron irradiation on the photosensitivity with measurements from an EG&G C30719F APD. The calculated fall in photosensitivity, from the model, is entirely due to the reduction of gain in the device. The measured reduction in photosensitivity cannot be explained by the fall in gain alone. The discrepancy is thought to be due to surface damage of the APD from the gamma background present during the neutron irradiation, an effect not included in the model. For

the longest wavelengths, where photon absorption beyond the gain region occurs, the reduction in photosensitivity is smaller because the fall in gain affects only part of the incident signal. Loss of red response due to diffusion effects, as in solar cells [24], is not expected as the device is almost fully depleted when operated normally.

VI. CONCLUSION

A 1-D device model allowing steady-state analysis of avalanche photodiodes has been developed and tested. The model follows the methodology proposed by Kurata [6] and includes several new features that allow accurate simulation of APD's. Impact ionization was included via a generation term in the continuity equations. The ionization rates for electrons and holes in silicon were used to describe the process. A modified form of the Baraff three-parameter theory was used to calculate the ionization rates. Illumination was incorporated by the inclusion of a generation term in the continuity equations which described the photoelectric generation of signal charge. 1 MeV neutron radiation damage was included via the introduction of deep acceptor levels subject to Shockley–Read–Hall statistics. A similar method using a Fermi occupancy function was used to accurately describe the change in N_{eff} with neutron fluence [16]. The lifetime damage-constant was used to describe the change in minority carrier life-time with neutron fluence. A value of $K_{\tau} = 10^7 \text{ scm}^{-2}$ was used for high resistivity-silicon. The effective lifetime in the depletion region was assumed to be the same. A trap, corresponding to the V_2O complex, was introduced at a rate of 0.96 cm^{-1} , following [17].

Preliminary analysis of an EG&G reverse reach through APD type C30626E was performed in which the gain and photosensitivity were investigated. Qualitative comparison was made with measurements performed on a commercial EG&G C30719F reverse reach through APD. The wavelength dependence of the gain, due to absorption of signal charge in the gain region, was well described by the model. The effects of neutron irradiation were also investigated. The most significant effect was the fall in gain during irradiation. This was attributed to a reduction in the electric field in the gain region due to negative space charge from the filled acceptor levels. The predicted fall in photosensitivity was found to be completely described by the fall in gain. This contradicted the measured results, which showed a fall in the photosensitivity that could not be described by the fall in gain alone. The discrepancy was thought to be due to surface damage caused by the gamma background during the neutron irradiation.

The initial results indicate that the model can be used as a useful tool in the analysis of silicon photodetectors for the LHC. The versatility of the model ensures that modification of different structures is simple. Further investigation of similar structures will be made to test its predictive power.

ACKNOWLEDGMENT

The authors thank D. Imrie and A. Holmes-Siedle for their careful scrutiny of this manuscript.

REFERENCES

- [1] F. Nessi-Tedaldi, "The CMS electromagnetic calorimeter," *Nucl. Phys. B (Proc. Suppl.)*, vol. 61B, pp. 52–58, Feb. 1998.
- [2] J. P. Pansart, "Avalanche photodiodes for particle detection," *Nucl. Instrum. Meth. A*, vol. 387, pp. 186–193, 1997. For example see.
- [3] T. Kirn *et al.*, "Wavelength dependence of avalanche photodiode (APD) parameters," *Nucl. Instrum. Meth. A*, vol. 387, pp. 202–204, 1997.
- [4] A. Karar, Y. Musienko, and J. C. Vanel, "Characterisation of avalanche photodiodes for calorimetry applications," *Nucl. Instr. Meth. A*, vol. 428, pp. 413–431, 1999.
- [5] R. J. McIntyre, P. P. Webb, and H. Dautet, "A short wavelength selective reach through avalanche photodiode," *IEEE Trans. Nucl. Sci.*, vol. 34, p. 1362–, June 1996.
- [6] M. Kurata, *Numerical Analysis for Semiconductor Devices*. Lexington, MA: Lexington, 1985.
- [7] B. Tuck, *Introduction to Diffusion in Semiconductors*. Stevenage, U.K.: Peregrinus, 1974.
- [8] D. L. Scharfetter and H. K. Gummel, "Large signal analysis of a silicon read diode oscillator," *IEEE Trans. Electron Devices*, vol. ED-16, pp. 64–77, Jan. 1969.
- [9] C. R. Crowell and S. M. Sze, "Temperature dependence of avalanche multiplication in semiconductors," *Appl. Phys. Lett.*, vol. 9, pp. 242–244, 1966.
- [10] G. A. Baraff, "Distribution junctions and ionization rates for hot electrons in semiconductors," *Phys. Rev.*, vol. 128, pp. 2507–2517, 1962.
- [11] A. D. Sutherland, "An improved fit to Baraff's universal curves for the ionization coefficients of electron and hole multiplication in semiconductors," *IEEE Trans. Electron Devices*, vol. ED-27, pp. 1299–1301, July 1980.
- [12] C. A. Lee and R. A. Logan *et al.*, "Ionization rates of electrons and holes in silicon," *Phys. Rev.*, vol. 134, pp. A761–A773, 1964.
- [13] J. Conradi, "Temperature effects in silicon avalanche photodiodes," *Solid-State Electron.*, vol. 17, pp. 705–718, 1974.
- [14] S. M. Sze, *Physics of Semiconductor Devices*, New York: Wiley, 1981.
- [15] W. C. Dash and R. Newman, "Intrinsic optical absorption in single crystal germanium and silicon at 77 K and 300 K," *Phys. Rev.*, vol. 99, pp. 1151–1157, 1955.
- [16] J. Matheson, M. S. Robbins, and S. J. Watts, "The effect of radiation induced defects on the performance of high resistivity silicon diodes," *Nucl. Instrum. Meth. A*, vol. 377, pp. 224–227, 1996.
- [17] S. J. Watts *et al.*, "A new model for generation-recombination in silicon depletion regions after neutron irradiation," *IEEE Trans. Nucl. Sci.*, vol. 43, pp. 2587–2594, Dec. 1996.
- [18] K. Gill, "Bulk damage effects in irradiated silicon detectors due to clustered divacancies," *J. Appl. Phys.*, vol. 82, pp. 126–136, July 1997.
- [19] F. Lemeilleur *et al.*, "Electrical properties and charge collection efficiency for neutron irradiated P-type and N-type Si detectors," *Nucl. Phys. B (Proc. Suppl.)*, vol. 32, pp. 415–424, May 1993.
- [20] J. Matheson *et al.*, "A microscopic explanation for type in version and the annealing behavior of radiation damaged silicon detectors," *Nucl. Instrum. Meth. A*, vol. 371, pp. 575–577, 1996.
- [21] B. C. MacEvoy, G. Hall, and K. Gill, "Defect evolution in irradiated silicon detector material," *Nucl. Instrum. Meth. A*, vol. 374, pp. 12–26, 1996.
- [22] G. Messenger, "A two level model for lifetime reduction processes in neutron irradiated silicon and germanium," *IEEE Trans. Nucl. Sci.*, vol. 14, pp. 88–102, Dec. 1967.
- [23] S. Baccaro *et al.*, "Radiation damage effect on avalanche photodiodes," *Nucl. Instrum. Meth. A*, vol. 426, pp. 206–211, 1999.
- [24] *Handbook of Space-Radiation Effects on Solar-Cell Power Systems*, NASA SP-3003, 1963.

Mark D. Osborne was born in Aldershot, U.K., on July 7, 1975. He received the B.Sc. degree in physics from Brunel University, Uxbridge, U.K., in 1996. He is currently pursuing the Ph.D. degree on the simulation of neutron radiation effects in avalanche photodiodes at Brunel University.

He is a member of the International Compact Muon Solenoid Collaboration.

Peter R. Hobson was born in Edinburgh, U.K., in 1959. He received the B.Sc. degree in physics from the University of Edinburgh, Edinburgh, U.K., in 1981, and the Ph.D. degree in physics from University College London, London, U.K., in 1985.

Since 1986, he has been a Member of the Permanent Academic Staff at Brunel University, Uxbridge, U.K. He was trained as a high-energy particle physicist and has devoted much of his research time to the development and exploitation of particle detector techniques for calorimetry. He is currently a member of the International Compact Muon Solenoid Collaboration, and is working on an electromagnetic calorimeter using lead tungstate crystals and vacuum phototriode light detectors. He is also active in precision holographic metrology, and has made contributions to the science and application of cerium-doped heavy-metal fluoride glasses. He has authored or co-authored nearly 200 research papers.

Stephen J. Watts was born in Ashford, U.K., in 1954. He obtained the B.Sc. degree in physics and the Ph.D. degree in experimental physics, both from London University, London, U.K., in 1972 and 1980, respectively.

He was appointed a Lecturer at Brunel University, Uxbridge, U.K., in 1985. He was promoted to Reader in 1990 and Professor in 1998. He is currently Head of the Electronic and Computer Engineering Department at Brunel University and leads the Sensors, Instrumentation and Radiation Effects group. His expertise is in radiation effects in silicon devices. He has published over 100 scientific papers to date.